A&A 379, 755–766 (2001)
DOI: 10.1051/0004-6361:20011232

Astronomy & Astrophysics

Radio monitoring of a sample of X– and γ–ray loud blazars⋆

T. Venturi[1], D. Dallacasa[2], A. Orfei[1], M. Bondi[1], R. Fanti[1,3], L. Gregorini[1,3], F. Mantovani[1], C. Stanghellini[4], C. Trigilio[4], and G. Umana[4]

[1] Istituto di Radioastronomia del CNR, Via Gobetti 101, 40129 Bologna, Italy
[2] Dipartimento di Astronomia, Bologna University, Via Ranzani 1, 40127 Bologna, Italy
[3] Dipartimento di Fisica, Bologna University, Via Irnerio, 46, 40126 Bologna, Italy
[4] Istituto di Radioastronomia del CNR, CP 141, Noto (SR), Italy

Received 25 June 2001 / Accepted 28 August 2001

Abstract. In this paper we present the results of a 4-year (1996–1999) radio flux density monitoring program for a sample of X– and γ–ray loud blazars. Our program started in January 1996 and was carried out on a monthly basis at the frequencies of 5 GHz and 8.4 GHz with the 32-m antennas located at Medicina (Bologna, Italy) and Noto (Siracusa, Italy). 22 GHz data collected at Medicina from January 1996 to June 1997 will also be presented. The sample of selected sources comprises most radio-loud blazars with $\delta \geq -10^{\circ}$ characterised by emission in the X– and γ–ray regimes, and target sources for the BeppoSAX X–ray mission. All sources in the sample, except J1653+397 (MKN 501), are variable during the four years of our monitoring program. We classified the type of variability in each source by means of a structure-function analysis. We also computed the spectral index $\alpha_5^{8.4}$ for all epochs with nearly simultaneous observations at these two frequencies, and found that $\alpha_5^{8.4}$ starts flattening at the very beginning of a radio flare, or flux density increase.

Key words. quasars – BL Lac objects – methods: observational

1. Introduction

The flux density variability of compact extragalactic radio sources is a well-established phenomenon, which can be explained as being due to the propagation of shocks in relativistic jets aligned close to the observer's line of sight (see for example Marscher & Gear 1985). The large amount of data available over a wide range of radio frequencies, makes it clear that different behaviours for the radio variability in blazars exist, and many different classes of spectral variability can be identified (for a review see Marscher 1993 and Wagner & Witzell 1995, and references therein).

The variability of blazars at X– and γ–ray energies is not as well documented as the radio flux density variability, however a study of simultaneous X–ray and radio–infrared flares has been reported for a few objects. Some examples include 3C279 (Maraschi et al. 1994; Wehrle et al. 1998), BL Lac (Kawai et al. 1991), NRAO 140 (Marscher 1988), PKS 2255−282 (Tornikoski et al. 1999), MRK 501 (Petry et al. 2000).

There are at present two main models accounting for the correlation observed. In the accelerating jet model (Maraschi et al. 1992) the synchrotron emission at UV, optical and IR frequencies is confined to the region closest to the central engine, opaque to the radio emission. The radio emission is produced outside this region, with the maximum intensity occurring where the Lorentz factor Γ is highest. Following this model, self-Compton scattered γ– and X–rays are produced in coincidence with the synchrotron emission in the UV, optical and IR bands closest to the central engine and in the radio core. Moreover, Inverse Compton reflection of optical and UV photons produced by the accretion disk would take place in the vicinity of the central engine, again producing X– and γ–ray emission. In a model consisting of a decelerating flow of relativistic positrons and electrons (Melia & Konigl 1989) the UV photons produced by the accretion disk are upscattered to X– and γ–ray energies. Radio and infrared synchrotron emission (plus self-Compton scattered X– and γ–ray emission) is produced where the Lorentz factor decreases down to a value of ∼10. Both models connect the emission in the different energy bands, and the location along the jet where the emission takes place, so in principle

Send offprint requests to: T. Venturi,
e-mail: tventuri@ira.bo.cnr.it

⋆ Table 3 is only available in electronic form at the CDS via anonymous ftp to cdsarc.u-strasbg.fr (130.79.128.5) or via
http://cdsweb.u-strasbg.fr/cgi-bin/qcat?J/A+A/379/755

it should be possible to discriminate between models and throw some light on the nature of the inner jets in blazars by means of multifrequency observations (Marscher 1993).

In order to increase the number of blazars (i.e. BL Lacertae objects, optically violent variables, high and low polarisation quasars) with multifrequency studies, we selected a sample of 23 radio-loud X– and γ–ray blazars, targets of X–ray observations carried out with the satellite BeppoSAX, and observed them at centimeter wavelengths on a monthly basis, for comparison with the results of the BeppoSAX X–ray mission. Our aim was to observe all sources in our list to provide radio lightcurves with very good and regular time coverage, which is crucial for an accurate multifrequency study of their variability. The desire for simultaneous (or nearly simultaneous) observations in the various bands is a result of the very high variability of these sources over the whole electromagnetic spectrum, and of the physical process responsible for the radio emission.

We report the source list, the description of the adopted observing strategy and the results in Sect. 2. A brief analysis of the variability and of the spectral index behaviour for all sources in the sample will be given in Sect. 3.

2. Source selection and observations

2.1. The sample of radio loud γ–ray blazars

The objects in our sample were selected from the list of steep spectrum and flat spectrum X–ray blazars, targets of observations with the X–ray satellite BeppoSAX. We chose all blazars with $\delta \geq -10^\circ$ with radio flux density $S \geq 1$ Jy at 5 GHz at the time we started our program. We point out that because of the strong variability of this class of sources, the list of selected objects cannot be considered complete.

Our sample includes 23 radio sources, reported in Table 1 with the most relevant information, i.e. J2000 and B1950 IAU name (Col. 1); alternative name (Col. 2); accurate J2000 radio coordinates taken from the VLA calibrator list (Cols. 3 and 4); redshift (Col. 5); optical ID (Col. 6). All sources in our list are part of the UMRAO database, see for example Aller et al. (1985) and the web page address: `http://www.astro.lsa.umich.edu/obs/radiotel/umrao.html` and have been monitored since the early seventies at centimeter wavelengths. However, our monitoring program, presented in the next section, does not duplicate but complements the major observational effort of the University of Michigan Radio Astronomy Observatory, especially in the light of the multiband analysis which motivated our observational project.
Five sources in our list were monitored with the Green Bank Interferometer at 8.4 GHz and 2.7 GHz until October 2000. Lightcurves and flux densities are available on the web at the: `http://www.gb.nrao.edu/fgdocs/gbi/gbint.html`

2.2. Observational strategy, data reduction and results

We started our monthly monitoring program at 8.4 GHz (3.6 cm) and 5 GHz (6 cm) in January 1996. All the 8.4 GHz observations were carried out with the 32-m antenna located at Medicina (Bologna, Italy); the 5 GHz observations prior to October 1997 were carried out with the 32-m antenna located at Noto (Siracusa, Italy), while the later 5 GHz observations were carried out at Medicina. The observations at 5 GHz and 8.4 GHz after this date were typically carried out within a few days of one another. The gap in the 8.4 GHz data, from June to November 1996, is due to the antenna track repair in Medicina. We present here also 22 GHz (1.3 cm) observations carried out in 1996 and part of 1997 at Medicina for the same set of sources.

Both left and right circular polarisation were recorded at Medicina, with a bandwidth of 80 MHz around the central frequencies 4967 MHz, 8447 MHz and 22 331 MHz. Total band observations, i.e. 4700–5050 MHz, were carried out at Noto, where only the left circular polarisation was recorded. The features of the antenna and of the cooled receivers at these frequencies are reported in Table 2, where we give the half power beamwidth ($HPBW$), the peak gain (g) and the receiver temperature system at the zenith ($T_{\rm sys}$) at each observing frequency. We note that the zenith $T_{\rm sys}$ includes also the sky.

In order to account for the local background, the data acquisition was performed with the on-source/off-source method, by means of the program ON−OFF. The off-source measurements were done with 5 beams off-source (on both sides of the source), in the azimuth direction. The duration of each ON−OFF cycle varied from 15 min for the strongest sources to 75 min for the weakest, which implies an effective integration time on source ranging from ∼3 to ∼15 min if we take into account all phases of the cycle.

DR21 was used as the primary calibrator at both frequencies, with adopted flux densities of $S_{5\,\rm GHz} = 22.5$ Jy (Baars et al. 1977) and $S_{8.4\,\rm GHz} = 21.5$ Jy (Ott et al. 1994), $S_{22\,\rm GHz} = 17.0$ Jy (Baars et al. 1977). We observed it 6−7 times during each observing run, in the range of elevations of 20°−85°. 3C 123, 3C 286 and 3C 274 were used as secondary calibrators and were observed twice each run.

The data reduction was carried out for the two polarisations independently using the program CINDY (Sanfilippo et al. 1995), written specifically for "single dish" observations. The antenna temperature on source $T_{\rm ant}$, derived on the basis of the on-source and off-source measurements, is transformed into flux density S by means of the formula: $S = T_{\rm ant}/G(z)$, where $G(z)$ is the antenna gain as a function of the source zenith angle. The data points were averaged to obtain a single flux density value, and the flux densities from the two polarisations were subsequently averaged together. We assumed no flux density variations during each observation.

Table 1. The radio sources.

IAU Name		Other Name	RA (J2000)	DEC (J2000)	z	Opt. ID
J0050−094	0048−097		00 50 41.32	−09 29 05.2	-	BL-Lac
J0238+166	0235+164		02 38 38.93	16 36 59.3	0.940	BL-Lac
J0530+135	0528+134		05 30 56.42	13 31 55.1	2.060	QSO
J0721+713	0716+714		07 21 53.45	71 20 36.4	-	QSO
J0738+177	0735+178		07 38 07.39	17 42 18.9	0.424	BL-Lac
J0841+708	0836+710		08 41 24.37	70 53 42.2	2.172	QSO
J0854+201	0851+202	OJ 287	08 54 48.87	20 06 30.6	0.306	BL-Lac
J0958+655	0954+658		09 58 47.25	65 33 54.8	0.368	BL-Lac
J1104+382	1101+384	MKN 421	11 04 27.31	38 12 31.8	0.030	BL-Lac
J1229+020	1226+023	3C 273	12 29 06.70	02 03 08.6	0.158	QSO
J1256−057	1253−055	3C 279	12 56 11.17	−05 47 21.5	0.536	QSO
J1419+543	1418+546	OQ 530	14 19 46.60	54 23 14.8	0.151	BL-Lac
J1512−090	1510−089		15 12 50.53	−09 05 59.8	0.360	QSO
J1653+397	1652+398	MKN 501	16 53 52.22	39 45 36.6	0.034	BL-Lac
J1748+700	1749+701		17 48 32.84	70 05 50.8	0.770	BL-Lac
J1751+096	1749+096		17 51 32.82	09 39 00.7	0.322	BL-Lac
J1800+784	1803+784		18 00 45.68	78 28 04.0	0.680	BL-Lac
J1806+698	1807+698	3C 371	18 06 50.68	69 49 28.1	0.051	BL-Lac
J1824+568	1823+568	4C 56.27	18 24 07.07	56 51 01.5	0.664	BL-Lac
J2005+778	2007+777		20 05 30.99	77 52 43.2	0.342	BL-Lac
J2202+422	2200+420	BL Lac	22 02 43.29	42 16 39.9	0.069	BL-Lac
J2232+117	2230+114	CTA 102	22 32 36.41	11 43 50.9	1.037	QSO
J2253+161	2251+158	3C 454.3	22 53 57.75	16 08 53.6	0.859	QSO

Table 2. Parameters of the observations.

Antenna	ν	Obs. Period	$HPBW$	g (L, R)	$T_{\rm sys}$ (L, R)
	MHz	mm/yy	arcmin	K/Jy	K
Medicina	4967	11/97–01/00	7.5	0.160 0.161	46 52
	8447	01/96–01/00	4.8	0.145 0.135	39 37
	22 331	01/96–06/97	2.0	0.116 0.118	120 120
Noto	4875	01/96–10/97	7.5	0.161	45

The calibration uncertainty in our data is of the order of 4% at all frequencies. This value was estimated comparing all the gain curves determined for each observing run. The expected thermal noise rms in our observations (see above and Table 2) is of the order of 2–5 mJy at 5 GHz and 8.4 GHz, and 6–15 mJy at 22 GHz. The most serious source of error in this type of observations is the uncertainty in the estimate of the atmospherical optical depth. The on-off procedure allows the subtraction of the "local" sky, therefore each individual point in the observations has already been corrected for this effect. We note, however, that the non-simultaneous measurements on- and off-source introduce an additional uncertainty, which we empirically estimated to increse the expected thermal noise by a factor of ∼4.

The results of our monitoring program are reported in Table 3, where we give the epoch and the flux density in Jy at 8.4 GHz, 5 GHz and 22 GHz. The error associated with each datapoint can be estimated following the indications given in the previous paragraphs with the simple formula:

$$\Delta S = 0.04 \times S + 4 \times \mathrm{rms}.$$

In Fig. 1 we show the lightcurves at all frequencies, and the spectral index between 8.4 GHz and 5 GHz for those epochs with time separation $\lesssim$7 days. The error bars in the plots take into account all the sources of error illustrated above.

Our data are in very good agreement with the flux density measurements provided by the UMRAO database for the common epochs. For the five sources included in the GBI sample, we found good consistency between ours and the GBI data.

3. Data analysis

3.1. Comments on the flux density variability

As is clear from Fig. 1 and Table 3, all sources in the sample show some degree of flux density variability at centimeter wavelengths during the four years of our monthly monitoring. The most quiescent source is J1653+397 (MKN 501), whose light curve remains almost flat both at 5 GHz and 8.4 GHz. From our data it is clear that the major outburst at X–ray energies detected for this source in 1997 did not propagate down to the radio regime covered by our observations (see also Petry et al. 1998).

Table 3. Flux density measurements (Sample page. The complete table can be found at the CDS).

Source	Date	S (Jy)	Date	S (Jy)	Date	S (Jy)
Var. Class	y m d	8.4 GHz	y m d	5 GHz	y m d	22 GHz
J0050−094	1996 01 30	1.42			1996 02 06	1.63
(b)	1996 03 04	1.63			1996 03 09	1.70
	1996 03 29	1.92	1996 04 15	1.29	1996 03 30	1.63
	1996 05 06	1.57				
	1996 05 24	1.52			1996 05 25	1.57
	1996 11 20	1.76	1996 11 13	1.60		
	1997 01 29	1.94	1997 02 06	1.43	1997 01 14	1.88
	1997 03 25	1.50			1997 03 22	1.19
	1997 04 15	1.38				
	1997 05 12	1.26				
	1997 06 20	1.41				
	1997 07 26	1.68				
	1997 08 01	1.70				
	1997 08 17	1.81	1997 10 11	1.60		
	1997 08 29	1.83	1997 12 24	1.54		
	1997 10 04	2.00	1998 01 14	1.22		
	1998 02 07	1.17	1998 02 04	1.13		
	1998 03 04	1.21	1998 03 07	1.00		
	1998 03 28	1.47				
	1998 05 07	1.55	1998 05 05	1.40		
	1998 06 27	1.45				
	1998 07 17	1.23				
	1998 07 29	1.17				
	1998 09 04	1.17	1998 08 31	1.06		
	1998 10 09	1.49	1998 10 02	1.33		
	1998 12 05	1.85	1998 12 07	1.62		
	1999 01 16	2.06	1999 01 05	1.91		
	1999 02 06	2.05				
	1999 05 05	1.42				
	1999 06 25	1.06				
	1999 07 15	1.03	1999 07 17	0.97		
	1999 07 22	1.02	1999 07 20	0.97		
	1999 08 18	1.22	1999 08 20	1.04		
	1999 10 07	1.16	1999 10 01	1.12		
	1999 11 06	1.19	1999 11 04	1.15		
	1999 12 06	1.36				
	2000 01 28	1.55	2000 01 10	0.95		

As discussed by Pian et al. (1997), the spectral properties of the 1997 flare and the major shift of the synchrotron peak, challenge most jet models.

We carried out a simple classification of the variability in all sources, applying a structure-function analysis (Hughes et al. 1992) to the 8.4 GHz observations. This dataset is the most complete among those presented in this paper, and for this reason it is particularly suited for this study.

The structure-function is defined as $SF(\tau) = < [S(t) - S(t+\tau)]^2 >$, where $S(t)$ is the flux at the time t and τ is the time lag. For an ideal process SF increases until it reaches a plateau, starting at a time $T_{\max}$, which corresponds to the timescale of the variability. The real cases, however, usually give more complicated structures.

We identified three different classes of variability, briefly described in the following paragraph. The variability class for each source is given in Col. 1 of Table 3. In Fig. 1, lower panel, we report the SF for each source.

Class (a) – Structure functions without a clearly defined plateau. This suggests that the time scale of the variability is longer than the duration of our monitoring. Examples in this class are J0530+135 and J1824+568 (4C 56.27). As visible from the light curve plots given in Fig. 1, some modulations are actually present in all these sources, however it is possible that their low amplitude compared to the global trend was missed by the analysis.

Class (b) – Structure functions with both maxima and minima. This case corresponds to recurrent variability, and the clearest examples are J0050−094, J1419+543 (OQ 530) and J1800+784. In all sources belonging to this class the amplitude of the variability is similar during the four years of monitoring.
Class (c) – Structure functions with one or more plateau. The first case, which includes for example J0238+166, identifies sources with one single outburst, while the presence of more than one plateau reflects the existence of different types of variability in the same source, such as for example in J0958+655, J1751+096 and J2253+161 (3C 454.3). In these sources short-term flux density fluctuations and longer-term variations seem to overlap. The majority of the sources in our sample belongs to this class.

We underline that there seems to be no difference in the structure function of quasars and BL Lacs, in that both populations include objects in each variability class.

Comparison of the flux density variability at 22 GHz, 8.4 GHz and 5 GHz in each source (see Fig. 1), indicates that not all sources in the sample show the same behaviour. In most cases the variability in these bands overlap, with simultaneous, or nearly simultaneous, maxima and minima. This is particularly clear for the recurrent variability of J0050−094, J1419+543 (OQ 530) and of J1800+784, but also for non-periodic variable sources such as J0530+135 and J1104+382 (MKN 421). In other cases, as for example J0238+166, J1229+020 (3C 273), J1256−057 (3C 279) and J1751+096, the flux density increase is visible first at higher frequencies, i.e. 22 GHz and 8.4 GHz, and subsequently propagates to 5 GHz. The time delay between the two frequencies seems to be of the order of a month for J0238+166 and J1751+096, and of the order of a few months for the other two sources.

One possible explanation to account for this result is that the mechanism responsible for the variability differs in the various cases. An analysis of the correlation between flux density variations and nuclear (i.e. parsec-scale) morphological changes was carried out by Zhou et al. (2000) for the blazar PKS 0420−014. For that source it was proposed that radio outbursts with a time delay going from high to low radio frequencies are due to intrinsic variations in the source nucleus, while simultaneous flares at different frequencies may be due to geometric effects. It would be important to carry out such an analysis for a larger sample of sources.

On the basis of the lightcurves derived from our monitoring program, a subsample of sources was selected for parsec-scale imaging and further investigation of their nuclear properties. In particular, J0050−094, J0238+166, J0958+655, J1512−090, J1751+096 were selected as representatives of different classes of variability (see the classification in Table 3), and multiepoch observations were carried out with the Very Long Baseline Array (VLBA) at 8.4 GHz and 22 GHz, yielding an angular resolution $\lesssim$1 mas. The observations were performed on 22 Jan. 1999 and on 7 Dec. 2000. In addition, J1512−090 was observed with the VLBA and the Space VLBI antenna HALCA on 11 Aug. 1999 and 13 May 2000, with a resolution comparable to that of the 22 GHz ground-array observations. J0050−094 and J0238+166 were found to be unresolved at both frequencies, while superluminal motion was found in J0958+655 and J1512−090, with implied Lorentz factors in the range 1.7–5. Preliminary results are presented in Venturi et al. (2000 and 2001), and further analysis is in progress (Venturi et al., in preparation).

3.2. Comments on the spectral index

The time coverage at 8.4 GHz and 5 GHz allowed the computation of the spectral index $\alpha_5^{8.4}$ for a number of epochs, especially starting from November 1997, when observations at both frequencies were carried out nearly simultaneously with the 32-m Medicina radio telescope. The trend of $\alpha_5^{8.4}$ versus epoch, to be read in the sense $S \propto \nu^{-\alpha}$, is reported in the bottom frame of the upper panel of Fig. 1 for each source.

As typical for compact radio sources, the spectral index is flat, i.e. $\alpha_5^{8.4} \sim 0$, or inverted in all cases, and it is mostly in the range $-0.5 \lesssim \alpha_5^{8.4} \lesssim 0$. The only two cases where $\alpha_5^{8.4} \gtrsim 0$ during the whole duration of our monitoring are J1653+397 (MKN 501) and J2253+161 (4C 454.3).

The spectral index usually starts steepening at the very beginning of a radio flare, or flux density increase, as is clear in particular for J0238+166 and J1229+020 (3C 273). This reflects the fact that the flux density increase takes place first at high frequencies, and/or that the amplitude of the flux density variations is on average more pronounced at 8.4 GHz.

4. Summary

We presented the results of a 4-year radio monitoring program carried out for 23 radio-loud blazars. In particular, the selected sources in the sample were monitored on a monthly basis at 8.4 GHz and 5 GHz, from January 1996 to January 2000. Observations at 22 GHz in the period January 1996 – June 1997 are also shown. The original aim was to provide good radio lightcurves for a set of blazars observed with the X–ray satellite SAX, for multiband analysis and to determine the spectral energy distribution (SED) from radio to X– and γ–ray energies for a larger number of such objects.

With the exception of J1653+397 (MKN 501), all sources in our sample showed some degree of variability during the period of the monitoring. A structure function analysis suggests that not all sources in the sample are characterised by the same type of variability. In some cases proper flux density flares are detected; in others recurrent variability is seen, and finally a more complicated behaviour is revealed in a number of sources, with flares of small amplitude superimposed on longer term variations. A detailed study of the lightcurves presented here will be done together with the X–ray data from BeppoSAX in a forthcoming paper. In particular, a thorough study and multiband analysis of the five sources imaged at parsec-scale resolution is in progress.

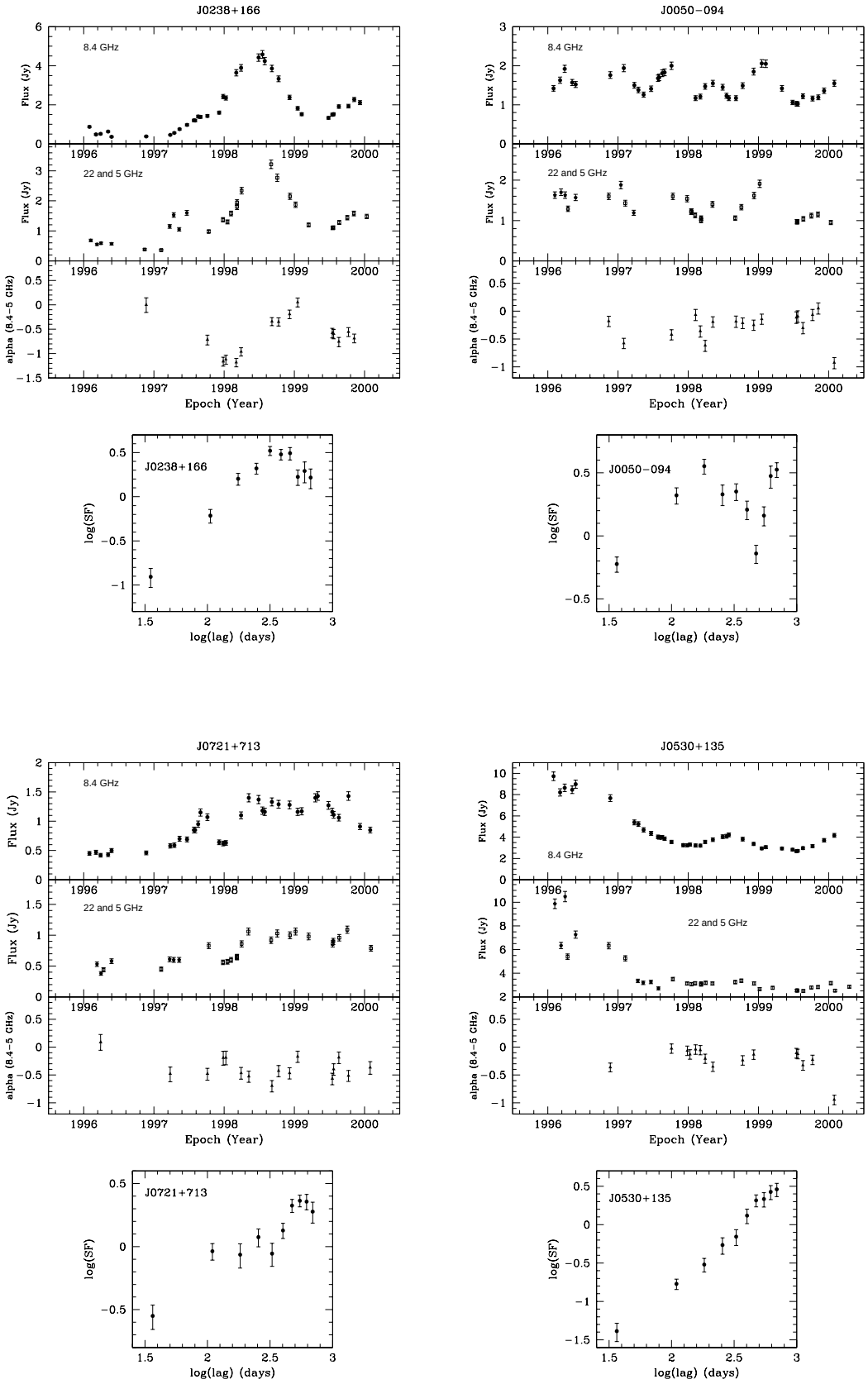

Fig. 1. For each source: upper panel – 8.4 GHz flux density curve data (upper frame); 22 GHz and 5 GHz flux density curves, shown respectively as filled pentagons and open squares (middle frame); spectral index $\alpha_5^{8.4}$ (lower frame). Lower panel – structure function derived on the basis of the 8.4 GHz data.

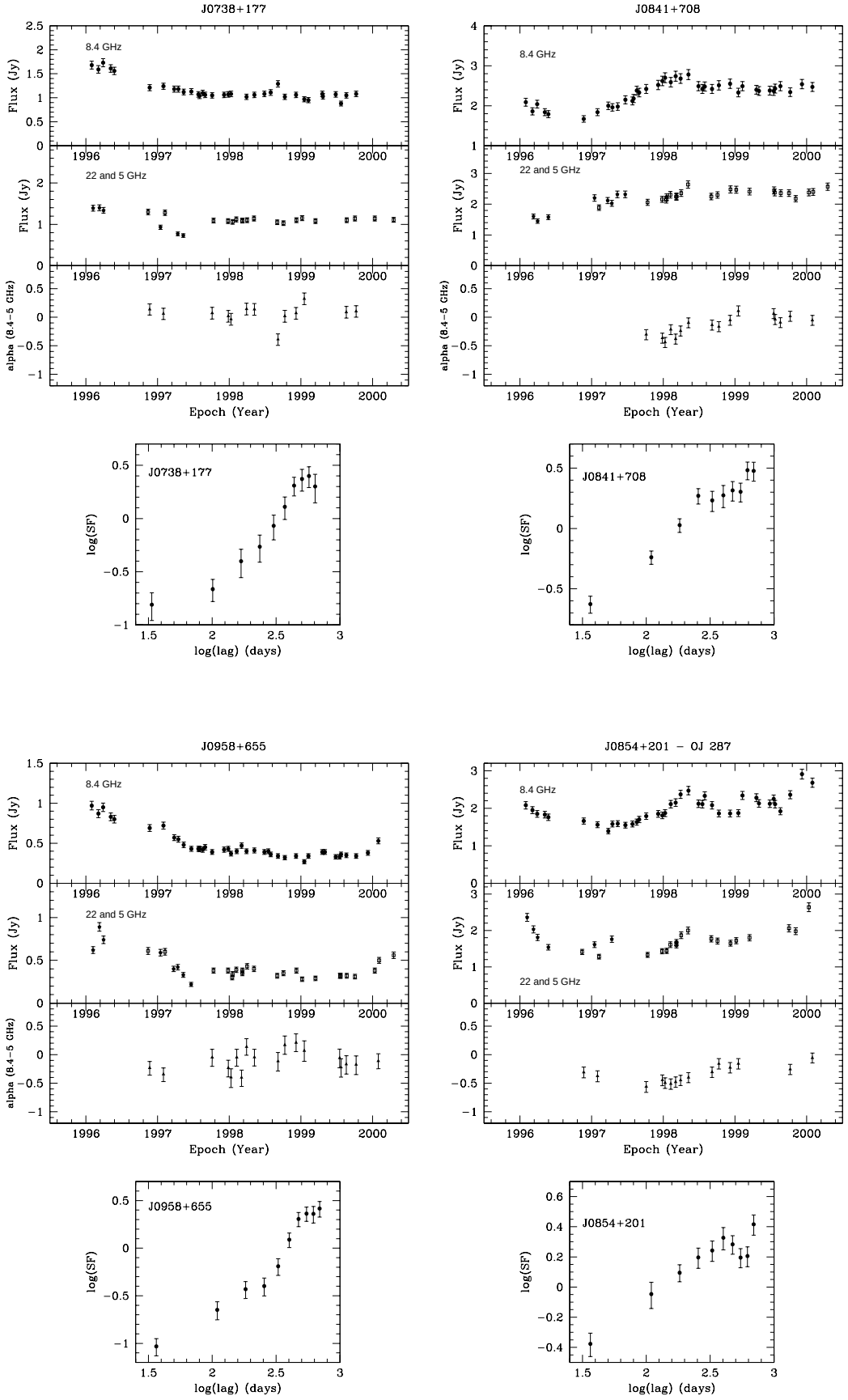

Fig. 1. continued.

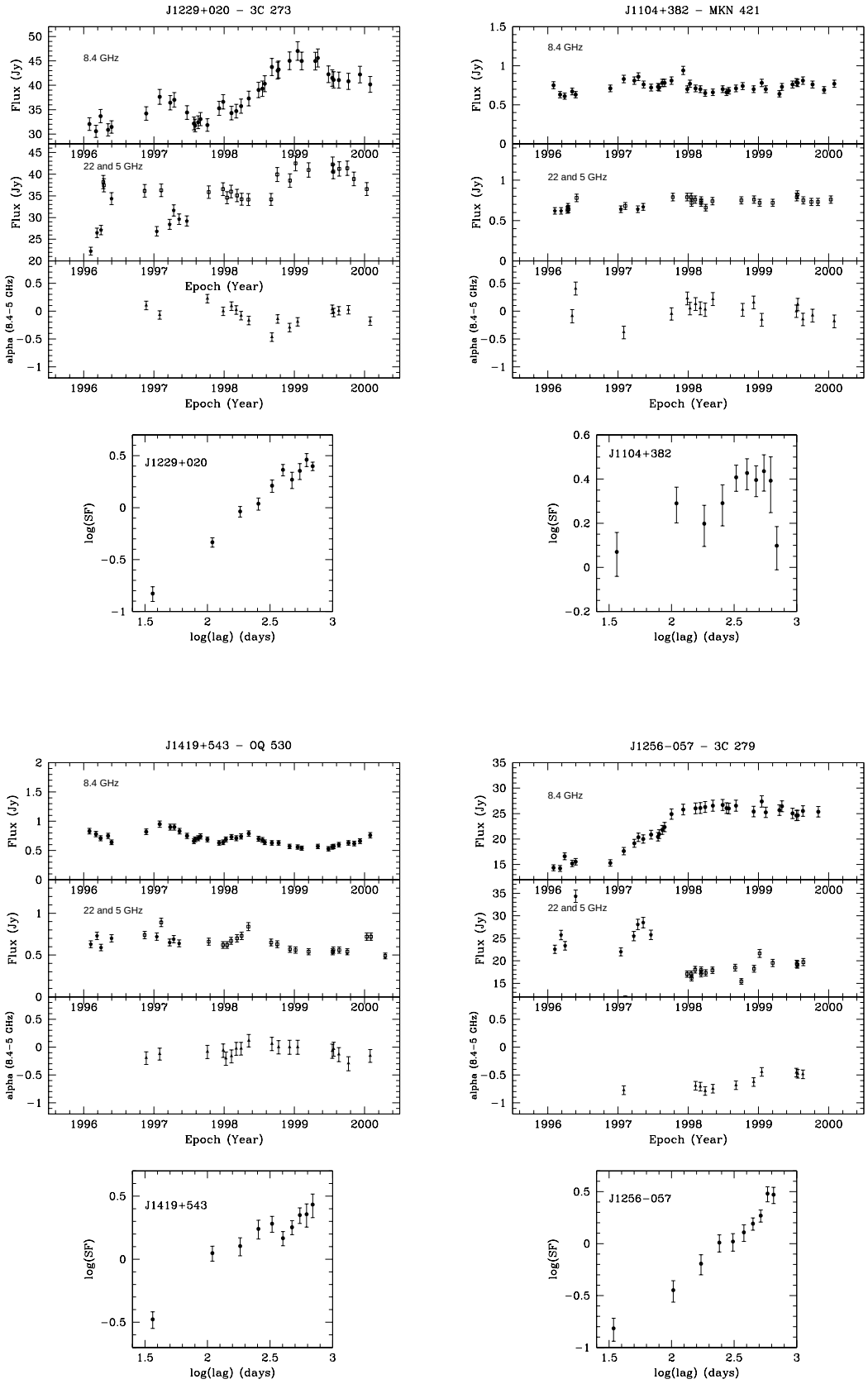

Fig. 1. continued.

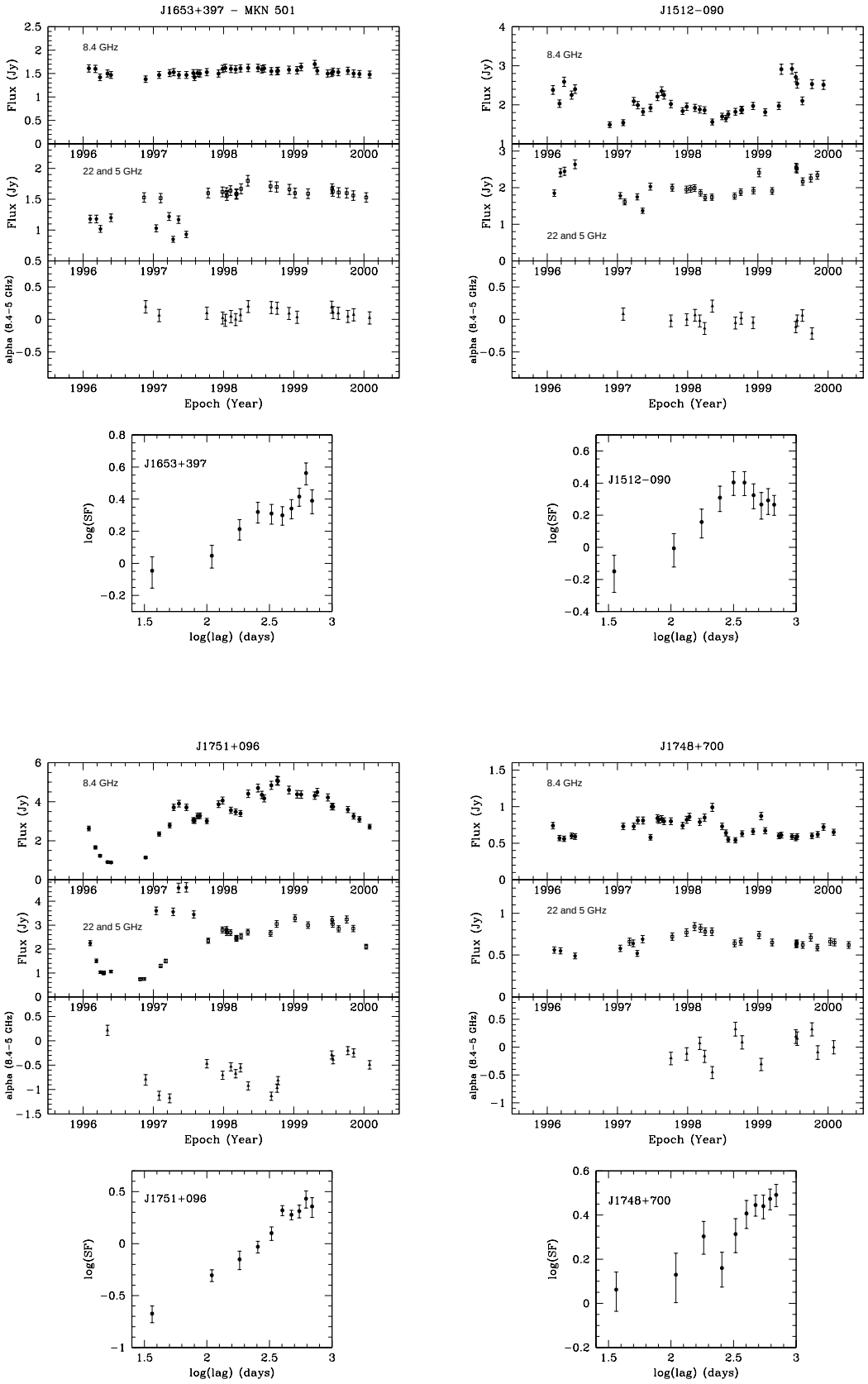

Fig. 1. continued.

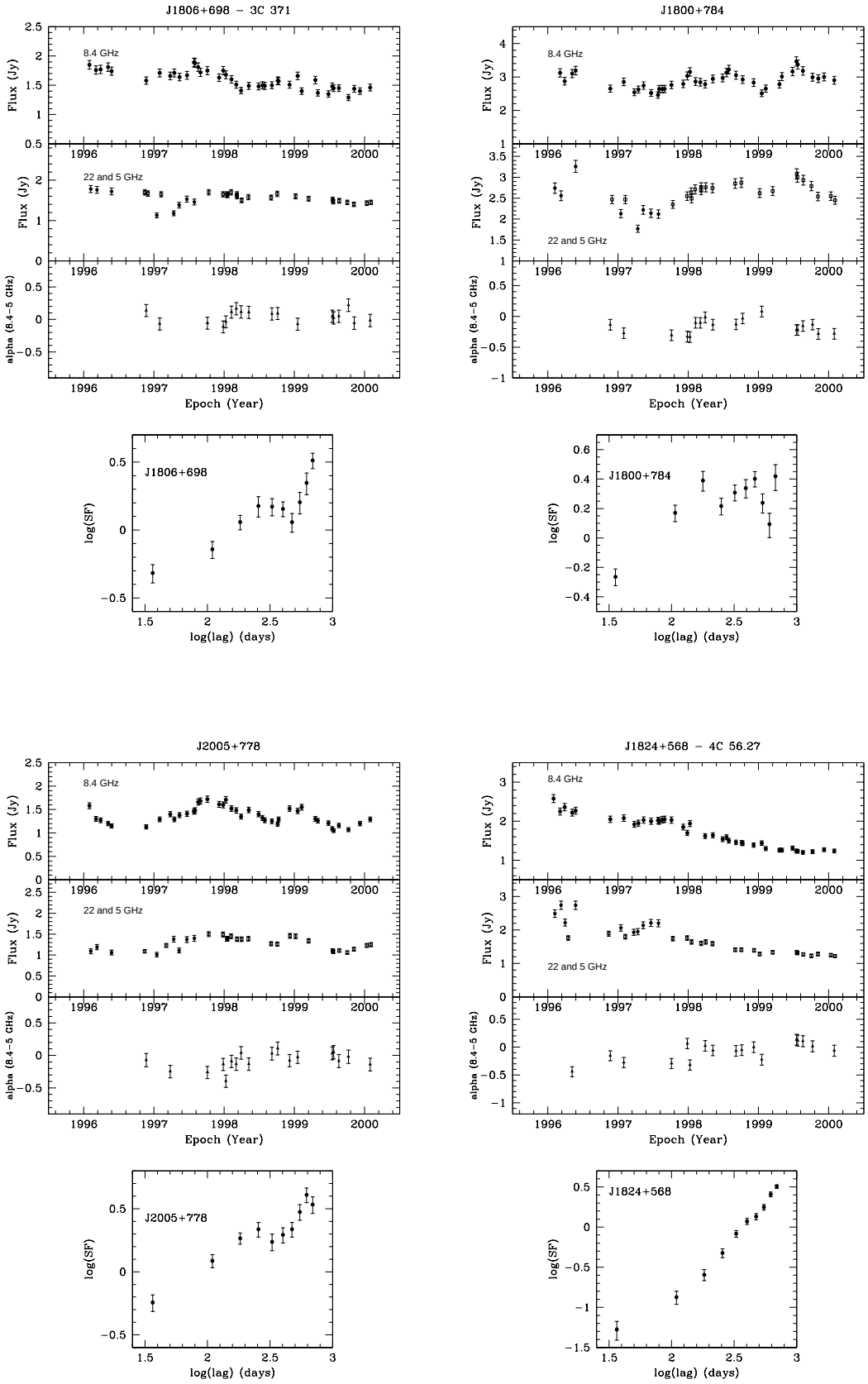

Fig. 1. continued.

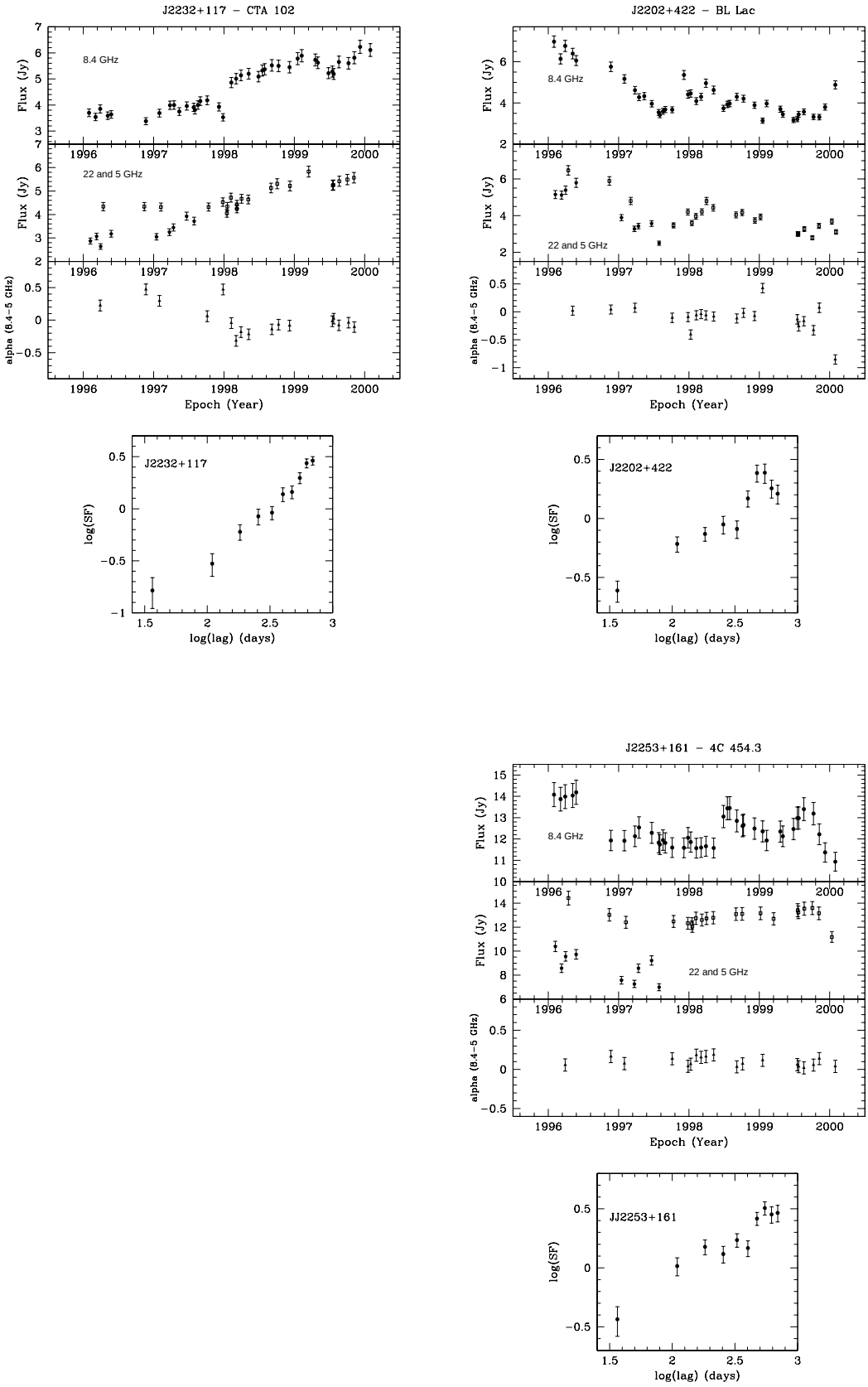

Fig. 1. continued.

Acknowledgements. This work has made use of the NASA/IPAC Extragalactic Database (NED), and of data from the University of Michigan Radio Astronomy, which is supported by the University of Michigan.

References

Aller, H. D., Aller, M. F., Latimer, G. E., & Hodge, P. 1985, ApJS, 59, 513
Baars, J. W. M., Genzel, R., Pauliny-Toth, I. I. K., & Witzel, A. 1977, A&A 61, 99
Hughes, P. A., Aller, H. D., & Aller, M. A. 1992, ApJ, 396 469
Kawai, N., Matsuoka, M., Bregman, J. N., et al. 1991, ApJ, 382, 508
Maraschi, L., Ghisellini, G., & Celotti, A. 1992, ApJ, 397, L5
Maraschi, L., Grandi, P., Urry, M. C., et al. 1994, ApJ, 435, L91
Marscher, A. P. 1988, ApJ, 334, 552
Marscher, A. P. 1993, in Astrophysical Jets, ed. D. Burgarella, M. Livio, & C. P. O'Dea (Cambridge Univ. Press, Cambrige), 73
Marscher, A. P., & Gear, W. K. 1985, ApJ, 298, 114
Melia, F., & Konigl, A. 1989, ApJ, 340, 162
Ott, M., Witzell, A., Quirrenbach, A., et al. 1994, A&A, 284, 331
Petry, D., Bottcher, M., Connaughton, V., et al. 2000, ApJ, 536, 742
Pian, E., Vacanti, G., Tagliaferri, G., et al. 1998, ApJ, 492, L17
Sanfilippo, D., Trigilio, C., & Umana, G. 1995, Rapporto Interno IRA, 215/95
Tornikoski, M., Tingay, S. J., Mücke, A., et al. 1999, AJ, 118, 1161
Venturi, T., Dallacasa, D., Torri, S., Mantovani, F. 2000, in Proceedings of the 5th European VLBI Network Symposium ed. J. E. Conway, A. G. Polatidis, R. S. Booth, & Y. M. Philström (Published by Onsala Space Observatory, Chalmers Technical University, Göteborg, Sweden), 45
Venturi, T., Dallacasa, D., Mantovani, F., & Torri, S. 2001, in Galaxies and their Constituents at the Highest Angular Resolution, ed. R. T. Schilizzi, S. Vogel, F. Paresce, & M. Elvis (Publish. Astron. Society of the Pacific), IAU Symp., 205, 142
Wagner, S. J., & Witzell, A. 1995, ARA&A, 33, 163
Wehrle, A. E., Pian, E., Urry, M. C., et al. 1998, ApJ, 497, 178
Zhou, J. F., Hong, X. Y., Jiang, D. R., & Venturi, T. 2000, ApJ, 541, L13